Advanced electrostatic model for monovalent ions based on *ab initio* energy decomposition

Zhifeng Jing, † Chengwen Liu, † and Pengyu Ren*

Department of Biomedical Engineering, The University of Texas at Austin, Austin, TX 78712

[†] Authors that contributed equally

^{*} Corresponding author. Email: pren@mail.utexas.edu

Abstract

Ions play important roles in the structures and functions of biomolecules. In biomolecular simulations, ions either directly interact with biomolecules or provide an ionic environment that influences electrostatic interactions of solutes. The AMOEBA+ water model has demonstrated significant advancement of classical force field for describing molecular interactions due to its improvements on the functional forms to account for essential physics. This work expands the applicability of the AMOEBA+ model towards alkali metal (Li, Na, K, Rb, and Cs) and halogen (F, Cl, Br, and I) ions. Various quantum chemical data on ion-ion and ion-water interactions, experimental ion hydration free energy, and lattice energy of salt crystals are used in the parametrization. The final parameters are verified with other properties outside of the parametrization data, including lattice energies of additional salt crystals and ionic activity coefficients in solution. The new models capture a wide range of ion properties from the gas phase to solution phase and crystals. More importantly, AMOEBA+ provides energy components that are consistent with ab initio energy decomposition. Thus we expect AMOEBA+ to be more general, transferable, and valuable for the interpretation of intermolecular forces in efficient classical simulations.

1. Introduction

Ions are critical to the structures and functions of biomolecules such as proteins, nucleic acids, and lipids. For example, ions participate in cellular signaling, conduction of neural impulses, osmotic pressure balance, enzymatic reactions, and many other processes. The monovalent sodium and potassium ions help maintain fluid and blood volume in the human body. The divalent magnesium is responsible for the catalytic functions of enzymes and structural stability of nucleic acids, while calcium modulates muscle contraction. Transition metal ions such as zinc and copper are generally considered necessary components of proteins, and their imbalance may lead to neurodegenerative diseases. However, computational modeling of the interaction between ions and biomolecules is challenging. Due to the high computational cost, quantum mechanical (QM) studies of biological systems are limited to either small model systems or computationally inexpensive approximations. Alternatively, simulations with classical molecular mechanical force fields can achieve reasonable accuracy and a much larger time and length scale.

A central ingredient of classical simulations is the underlying force field (FF) model that describes the interactions of the chemical species in a system. Developing FF models for ions has been an active research field due to their biological importance described above. The popular FF models, such as AMBER, CHARMM, and OPLS, all use Coulomb potential with fixed-pointcharge and empirical Lennard-Jones (LJ) potential to describe the interactions between ions and other molecules. The charges of ions in these models are set to integer numbers, which leads to only two tunable parameters (namely, the vdW size and the depth of potential well). Developments of classical ion models include special LJ parameters for cation-anion interactions⁶⁻⁷ and the LJ 12-6-4 potential (including ion-induced dispersion energy).⁸⁻⁹ Despite their simplicity and reasonable accuracy for biomolecular simulations, the limitations of these models are recognized in the literature. For example, these models have been shown incapable of describing the ion distribution at the air-water interface, ¹⁰ the ion aggregation at elevated temperature and pressure, ¹¹ and the specificity of ion-protein binding. 12 The explicit inclusion of polarization effect, via either Drude oscillator or induced point dipole scheme, helps tackle some of these issues. The polarization effect accounts for the electron response to the electrostatic field of ions and the environment. Drude polarizable FF has been parametrized in conjunction with SWM4-NDP water for atomic and molecular ions. 13-14 Ion LJ parameters were tuned to reproduce QM ion-water interaction energy and experimental hydration free energy (HFE). AMOEBA polarizable FF for atomic ions has also been developed by using a similar approach.¹⁵⁻¹⁶ These ion models have been used to study a variety of biological problems, such as ion permeation in membrane channels,¹⁷ ATPases,¹⁸ and ion selectivity in proteins.¹²

AMOEBA+ model improves on AMOEBA by including new energy functional terms to capture essential physics of molecular interactions. As described in the previous publication, ¹⁹ AMOEBA+ maintains the atomic multipole moments (charge, dipole, and quadrupoles) to represent the electrostatics. The original Thole damping scheme of AMOEBA *direct* induction has been modified to better capture the QM many-body interaction energy. ²⁰ Meanwhile, an improved combining rule for vdW, namely the "W-H" rule, has been adopted due to its ability to describe better the exchange-repulsion and dispersion interactions from QM energy decomposition analysis (EDA). ²¹ More importantly, AMOEBA+ incorporates new mathematical functions to describe charge penetration (CP), charge transfer (CT), and geometry-dependent charge flux (CF) effects. The total potential energy of a molecular system is composed of these terms described in Equation 1

$$E_{total} = E_{bonded} + E_{electrostatics} + E_{polarization} + E_{charge-transfer} + E_{vdw}$$
 (1) In the above equation, the bonded terms in AMOEBA+ are kept the same as those from the AMOEBA model.²² The buffered-14-7 function of Halgren²³ together with a modified combining rule (see ref. ²¹) is used for the E_{vdw} term. Detailed charge flux implementation in AMOEBA+ can be found in previous publications.²⁴⁻²⁵ We will describe the $E_{electrostatics}$ with CP correction, $E_{polarization}$ with improved damping scheme and $E_{charge-transfer}$ in the Method section below.

With the above improvements in functional forms, AMOEBA+ parameters for water have been developed by targeting QM energy data, interaction energy components, and reliable experimental data for liquid properties.²⁴ The model has been examined on selected properties of gas, liquid, and crystal phases. To expand the applicability of the AMOEBA+ model towards biomolecular systems, we performed the parametrization of monovalent metal ions (Li, Na, K, Rb, and Cs) and halogen ions (F, Cl, Br, and I) in this work. The new functional forms introduced in the AMOEBA+ model allow us to target extensive QM data and experimental properties in parametrization and validation. In parametrization, the extensive interaction energy of ion-ion and ion-water clusters is computed at the MP2 or CCSD(T) level of theory. Energy components from two energy decomposition analysis (EDA) approaches are used to parametrize the electrostatics interaction. Together with the QM total energy and EDA data, the experimental HFE of ions and

lattice energy of salt crystals are used in the parametrization. Finally, the optimized parameters are validated with ionic activity coefficient and additional crystal lattice energy data.

2. METHOD

In AMOEBA+, an atomic ion is defined by charge, charge penetration (CP), polarization, charge transfer, and vdW parameters. Same as in other models, a fixed charge of +1 or -1 e is assigned to each cation and anion, respectively. CP refers to the deviation of the intermolecular electrostatic interaction from a Coulomb potential between point multipoles. With the CP correction, the electrostatic potential due to a point charge in AMOEBA+ is expressed as

$$V_q = [Z_{\text{eff}} - (Z_{\text{eff}} - q)(1 - \exp(-\alpha_{\text{CP}}r))]/r$$
 (2)

where r is the distance from the atom; effective charge $Z_{\rm eff}$ and exponent $\alpha_{\rm CP}$ are tunable parameters.²⁶ The damping function $1 - \exp(-\alpha_{\rm CP} r)$ is applied to the electron charge $(Z_{\rm eff} - q)$ part. The damping functions accounting for higher order interactions can be found in our previous publication.²⁷ Polarization is represented by induced dipoles, which can be separated into a *direct* induction by permanent atomic multipoles and a *mutual* induction by other induced dipoles (the first and second terms of the right-hand side of Equation 3, respectively),

$$\mu_i^{\text{ind}} = \alpha_i \left(\sum_j T_{ij}^{\text{damped}} M_j + \sum_j T_{ij}^{\text{damped}} \mu_j^{\text{ind}} \right)$$

$$f_{\text{Thole}}(r) = 1 - e^{-au(r)^3}$$

$$f_{\text{MB}}^{\text{direct}}(r) = 1 - e^{-a^*u(r)^{3/2}}$$
(3)

where T_{ij} represents multipole-multipole interaction tensor (for *mutual* induction, it consists of dipoles only), M_j is the atomic multipole, α_i is the isotropic atomic polarizability, f is the damping function for either the *direct* induction or *mutual* induction, a and a^* are the damping factors for *direct* and *mutual* induction. The reason why a different damping function (other than Thole) is used for the direct induction, as described, is to better describe QM many-body (three- and four-body) energy.²⁰ Charge transfer energy between two atoms is represented by an exponential function,

$$E_{\text{CT},ij} = -A_{ij} \exp(-B_{ij}r_{ij}) \tag{4}$$

where the prefactor A and exponent B are parameters under determination.

In total, there are nine tunable parameters for each ion. For comparison, popular fixed charge FFs only require two vdW parameters, and AMOEBA only requires two vdW and two polarization parameters. If the parameters for each energy component can be determined independently, the parameter fitting will be significantly simplified. However, there is no unique way to separate charge transfer from polarization, and currently available methods, such as ALMO²⁸ and regularized SAPT,²⁹ could lead to unstable or unphysical charge-transfer energy.³⁰ In addition, force fields only need to predict accurately the total energy of a system. Although the accuracy for each energy component is helpful for improving transferability, the total energy should be prioritized when there is a conflict between the total energy and an energy component or the target data for the energy component is questionable.

Here, the total energy for ion-water dimers/clusters and ion pairs/trimers (Figure 1, Table 1), energy decomposition analyses from SAPT and ALMO, and experimental lattice energy and HFE were used to determine ion parameters. The SAPT2+ level of theory was used for all SAPT calculations.

Ion-water dimers. The optimized structures were either taken from the literature³¹ or obtained through geometry optimization at the MP2/aug-cc-pVTZ level. Then a rigid scan of the intermolecular distance (M-O or X-H) was performed by moving the ion along the M-O or X-H vector. A total of 13 data points for each dimer were generated with the distance ranging from $0.8 \times r_0$ to $3.0 \times r_0$, where r_0 is the distance in the optimized structure, or the equilibrium distance. The interactions were calculated by MP2/CBS/aug-cc-pV[T,Q]Z + δ CCSD(T)/aug-cc-pVTZ and SAPT/aug-cc-pVQZ. This scheme for geometry optimization and interaction energy was used for all other structures unless otherwise noted. The difference between CCSD(T)/CBS and SAPT2+/aug-cc-pVQZ are smaller than 0.5 kcal/mol in most cases except for F-. Counterpoise correction was applied for all MP2 and CCSD(T) interaction energy calculations. According to Lao et al., 31 def2-TZVPP or def2-QZVPP instead of aug-cc-pVTZ or aug-cc-pVQZ was used for

alkali metal and iodine. Unless otherwise noted, all the geometry optimizations were done on Gaussian16 ³² and energy calculations were done on Psi4. Frozen core was disabled for all calculations of cations.

Ion-water clusters. The ion-water clusters contain 2 to 6 water molecules. To sample the cluster configurations, we performed MD simulations of one ion solvated in a water box using the NVT ensemble at 298 K. Then 10 structures for each of the cluster size were extracted from the 2-ns MD trajectory. The structures were first optimized by MN15/aug-cc-pVDZ and then optimized by MP2/aug-cc-pVTZ. Gaussian was used for the MN15 optimization, while ORCA 4³³ and Psi4³⁴ packages were used for the MP2 optimization of Rb/Cs/I and other ions, respectively. Unique structures were selected based on the covariance matrix of the coordinates of ion and oxygen atoms. The interaction energy between the ion and the water molecules (rather than total interaction energy) was calculated by MP2/CBS/aug-cc-pV[T,Q]Z.

Ion dimers. The ion dimers include both homodimers and heterodimers. The geometries of cation-anion dimers were optimized by MP2 and the interactions were calculated by CCSD(T) and SAPT. The intermolecular distance for homodimers was varied from 0.9x to 1.2x the optimized distance in ion-water dimer. The distance for heterodimers was varied from $0.8 \times r_0$ to $3.0 \times r_0$.

Symmetric linear ion trimers. The geometries were optimized by a scan of the interatomic distance using MP2/aug-cc-pVTZ. The total interaction energy was calculated by CCSD(T), and the polarization energy was calculated by ALMO-EDA2 at the ωB97X-V/def2-QZVPPD level of theory. ALMO-EDA was used to calculate the polarization contribution, since SAPT does not separate polarization from charge transfer and does not support trimers. The accuracy of the ALMO polarization decomposition scheme has not been validated against other methods, so the polarization contribution is only for semi-quantitative comparison. Since AMOEBA+ polarization energy is negligible due to symmetry, the AMOEBA+ interaction energy was compared to the QM non-polarization energy. The symmetric linear ion trimers were included mainly for parameterization of charge transfer.

Salt crystals. Experimental lattice energy and lattice length were included in the target data. However, the numerical evaluation of derivatives for lattice length can be noisy. Instead of directly fitting to the lattice energy and lattice length, the lattice energy curve as a function of lattice length was used as the target, which is similar to the dimer interaction energy. The target lattice energies for off-equilibrium lattice lengths (±0.25 Å, ±0.5 Å) were generated by scaling the experimental lattice energy according to the AMOEBA lattice energy curve. Supercells containing 432 atoms for pcc crystals (CsCl, CsBr and CsI) and 512 atoms for fcc crystals were constructed. Only crystals containing Na and/or Cl were included in the target data, and other crystals were used for validation. Ewald summation was used to calculate the long-range electrostatics interactions.

The ion HFE was calculated by using periodic boxes and the standard free energy perturbation method as described in our previous work.^{3,35} The simulation box contained one ion solvated in water, with a volume of (37.3 Å)³ and a density of 1.0 g/cm³. Previous work showed that the ion HFE is not sensitive to system size from 500 to 4000 water molecules.³ The simulations were performed in the NVT ensemble at 298 K. The simulation time at each window was 1 ns and the coordinates were saved every 1 ps. Tinker-OpenMM³⁶⁻³⁷ was used for all MD simulations. While the HFE of an ion pair can be measured experimentally, the HFE of a single cation/anion depends on the HFE of proton, which does not have a unique value.⁵ The "intrinsic" HFE accounts for the interaction between ion and water, while the "real" HFE also includes the phase potential which amounts to 0.2-0.5 V.³⁸⁻³⁹ MD simulation results and the Schmid value are close to the intrinsic HFE, so the Schmid value was chosen as the target. This choice is consistent with previous work on ion models. ^{8-9, 15-16}

Ionic activity coefficient. The ionic activity coefficient was calculated by using the method described by Wang.⁴⁰ Briefly, the mean ionic activity coefficient γ_{\pm} is related to the ion HFE by Eq. (5)

$$\beta \Delta A_{\text{solv}} = 2 \ln \gamma_{\pm} + 2 \ln \left[\frac{\rho_{\text{w}}}{\rho_{\text{h}}} \left(1 + \frac{N_{\text{s}} M_{\text{s}}}{N_{\text{w}} M_{\text{w}}} \right) \right]$$
 (5)

where ρ_b and ρ_w are the densities of the solution and the solvent, N and M are the number and molar mass while the subscript s/w indicates solute/water. The HFE of the ion pair was calculated by using the standard protocol.^{3,35} The simulations were performed in the NPT ensemble at 298 K and 1 bar. Each free energy calculation contains 20 alchemical windows and 2 ns simulations at each window. 3 to 12 independent sets of simulations at each concentration were performed to reduce the statistical uncertainty. The box size was about (35 Å)³.

Table 1: Summary of target data for the derivation of ion parameters. M/X denotes cation/anion.

System	Comment	Properties
		1
Ion-water dimer	$M + H_2O, X + H_2O$	Total interaction energy
		Energy components
Ion-water cluster	M + $(H_2O)_n$,	Total interaction energy
	$X + (H_2O)_n, 2 \le n \le 6$	
Ion pair	M-X, M-M, X-X	Total interaction energy
		Energy components
Ion trimer	M-X-M	Total interaction energy
Salt crystal	Salts containing Na and/or	Lattice energy/length
_	Cl;	
	face centered cubic or	
	primitive cubic cell	

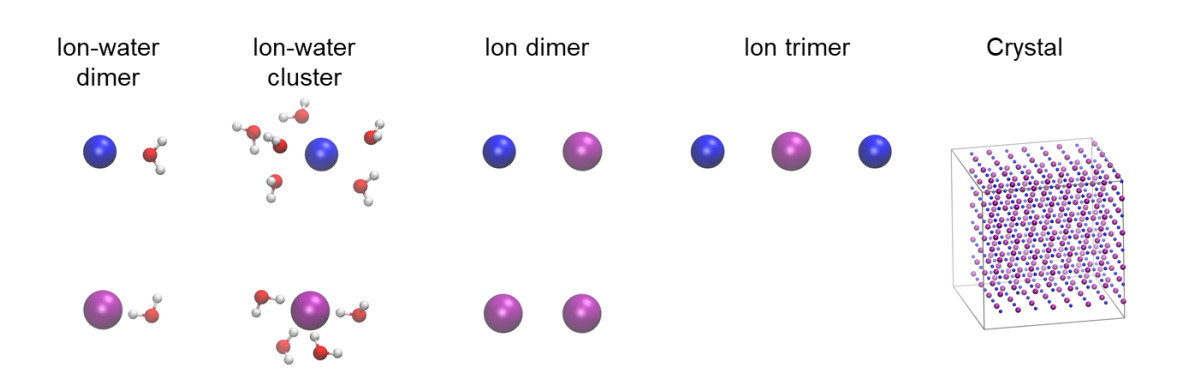


Figure 1: Examples of structures used in AMOEBA+ energy calculations. Blue and purple spheres represent cation and anion, respectively; red/white spheres represent O/H in water.

Parameter optimization. Because the dataset contains interactions between different ions, the parameters for each ion cannot be determined separately. Simultaneous optimization of all ions would be very slow and may lead to poor results since one objective function is used for a large parameter space. Here, the parameters were optimized in two steps. First, the parameters for the most common ions, Na+, K+, and Cl- were optimized together. Then the parameters for other ions were optimized separately using the data for ion-water interaction and ion-pair interaction between the target ion and Na+ or Cl-. For most ions, there is no need to optimize the effective charge. For Br- and I-, using the effective nuclear charge obtained from SCF calculations⁴¹ significantly improves the electrostatic energy. The atomic polarizability has a relatively small effect on the polarization energy, and it was determined from QM calculations on single atoms. When Na+, K+, and Cl- parameters are optimized together, there could be multiple optima. So the parameter space was explored by a scan of selected parameters, including polarization damping and charge-transfer exponent B. For other ions, only the polarization damping parameter was scanned. As a result, there were only 4 or 5 fitting parameters for each ion during optimization: vdW r_0 and ϵ , charge transfer A (and B for Na+, K+, Cl-), and charge penetration α_{CP} . In each optimization step, the objective function is a sum of squared errors for each property,

$$L(\mathbf{x}) = \sum_{i} w_{i} (A_{i}(\mathbf{x}) - A_{i}^{0})^{2} + \alpha \sum_{i} \left(\frac{x_{i} - x_{j}^{0}}{x_{j}^{0}}\right)^{2}$$
(6)

where A_i^0 is the target value for one property and A_i is the corresponding property predicted from the force field parameters \mathbf{x} , w_i is the weight for this property, x_j^0 and x_j are the initial and current values for the jth parameter, and α controls the overall weight of the regularization term. By convention, the parameters in the objective function α , w_i and u_j are referred to as hyperparameters. These hyperparameters can have a large influence on the optimization results. Any least-square optimization algorithm can efficiently minimize the objective function. Here the Trust Region Reflective algorithm as implemented in SciPy (https://scipy.org/) was chosen.

The weights were assigned based on the accuracy and importance of the reference data. For the QM data sets, the weights were calculated as the product of the relative weights between different sets (Table 2) and the weights within each data set (Table 3). Ion-water interactions were assigned larger weights than ion-ion interactions, and the ion linear trimers were assigned the smallest weights. Within each data sets, the weights were proportional to the inverse square of the error. The errors were calculated by

$$\sigma = \max\{0.1, |E_{aTZ} - E_{ref}|\} \text{ (kcal/mol)}$$
(7)

where E_{aTZ} is the energy calculated by either MP2 or SAPT with the aug-cc-pVTZ basis set, and E_{ref} is the reference energy with CBS or aug-cc-pVQZ basis set. The error in minimum interaction energy is about 0.3~1.0 kcal/mol for ion-water dimers and 1~3 kcal/mol for ion homodimers, heterodimers and trimers. In addition, the 3 data points with the lowest energy in the interaction energy curve were assigned 100x weights, which effectively incorporates the importance of the gradient near the minimum; the total interaction energy and the electrostatic energy were assigned 8x and 4x weights compared to other components, because the total interaction energy is more important, and the electrostatic energy is more reliable than other energy components. For the experimental data, the HFE was assigned similar weights as the ion-water interaction energies, while the lattice energy has smaller weights. A small regularization factor $\alpha = 1.5 \times (n_{data}/n_{parameter})^2$ was used so that the optimization results were not very sensitive to the initial parameters. The initial parameters were taken from previous AMOEBA^{15, 22} and AMOEBA+⁴² force fields. The optimized parameters are listed in Table 4.

Table 2. Relative weight between different QM data sets on ionic interactions.

Dataset	Relative weight
Ion-water dimer	1
Ion homodimer	1E-2
Ion heterodimer	1E-2
Ion linear trimer	1E-6
Ion-water cluster	1

Table 3. Weights for different types of QM and experimental data. σ is the estimated uncertainty.

Property	Weight
Dimer/trimer interaction energy, 3 lowest points	8E4 × $(\sigma/\text{kcal·mol}^{-1})^{-2}$
Dimer/trimer interaction energy, all except 3 lowest points	$8E2 \times (\sigma/\text{kcal·mol}^{-1})^{-2}$
Dimer electrostatic interaction energy	$4E2 \times (\sigma/\text{kcal·mol}^{-1})^{-2}$
Dimer vdW/induction interaction energy	$1E2 \times (\sigma/\text{kcal·mol}^{-1})^{-2}$
Ion-water cluster interaction energy	$8E2 \times (\sigma/\text{kcal·mol}^{-1})^{-2}$
Lattice energy	4
Hydration free energy	10 ⁴

Table 4: Optimized AMOEBA+ ion parameters.

ion	vdw		polarization		CT		CP		
		3		а	a*	A			
	σ (Å)	(kcal/mol)	α (Å ³)	(mutual)	(direct)	(10^3kcal/mol)	B (Å ⁻¹)	α_{CP}	$Z_{ m eff}$
Li+	1.91238	0.1214	0.028	0.39	0.25	0.1362	8.0000	97.0415	3.0
Na+	2.29371	1.1707	0.08	0.05	0.25	5.9675	2.8000	7.0067	11.0
K+	3.23764	0.9292	0.78	0.05	0.50	13.0744	3.0000	7.6694	19.0
Rb+	3.64298	0.6906	1.35	0.39	0.70	8.8769	3.0000	7.1575	37.0
Cs+	3.96943	0.7275	2.26	0.39	0.70	16.0675	3.2000	7.3729	55.0
F-	4.45376	0.0116	1.35	0.39	0.70	16.9753	7.2432	8.2761	9.0
Cl-	4.70814	0.1757	4.00	0.39	0.55	1.4695	2.5000	3.0400	17.0
Br-	5.02935	0.2014	5.65	0.39	0.70	10.7969	2.8257	2.3347	9.0
I-	5.27445	0.2777	7.25	0.39	0.70	9.2620	2.5029	2.3392	11.6

3. RESULTS

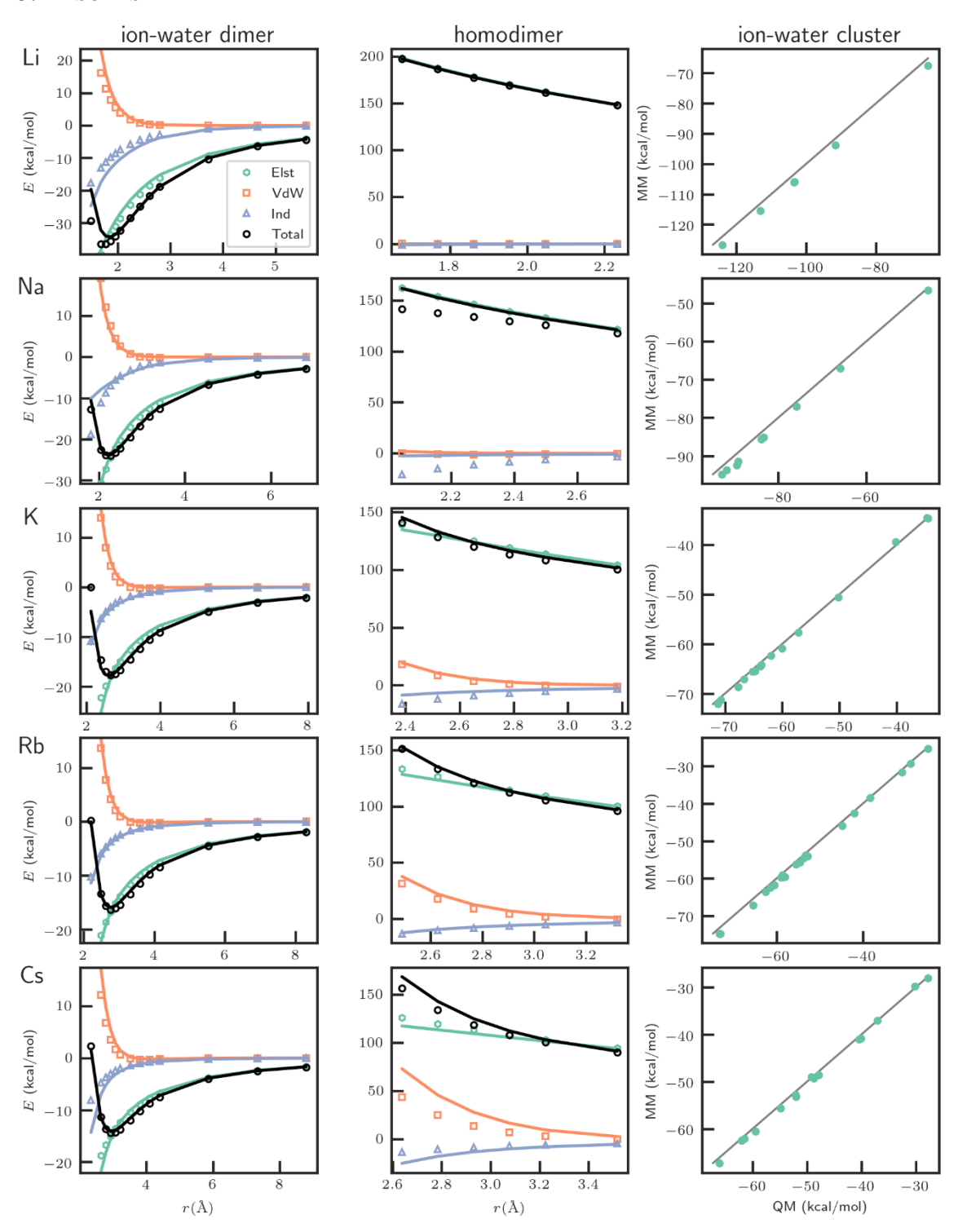


Figure 2: AMOEBA+ and QM interaction energies for Li, Na, K, Rb, and Cs. QM total interaction energy is calculated by CCSD(T)/CBS, while energy components are calculated by SAPT2+. "Elst" denotes electrostatics; "Ind" denotes induction, which is the total induction energy in SAPT or the sum of polarization and charge transfer energy in AMOEBA+. For ion-water dimer and homodimer, QM energy is represented as solid lines and MM energy is represented as hollow symbols.

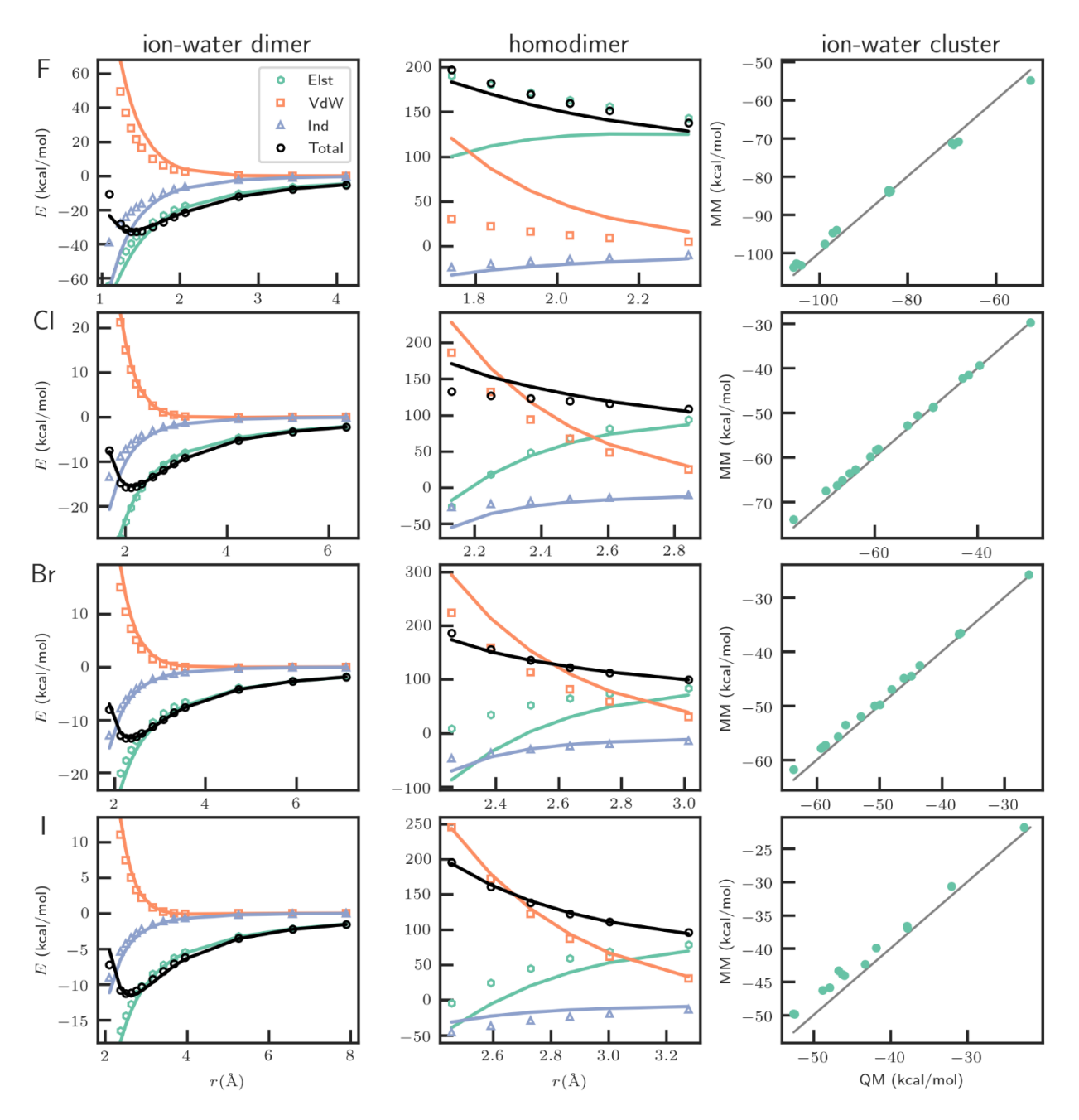


Figure 3: AMOEBA+ and QM interaction energies for F, Cl, Br, and I. QM total interaction energy is calculated by CCSD(T)/CBS, while energy components are calculated by SAPT2+. See Figure 2 caption for the description of the energy components.

The ion-water dimer and ion homodimer interactions were examined in Figure 2 and Figure 3. Ion-water dimer interaction is the most basic interaction for ions and the only gas-phase interaction used for the development of most ion models.¹⁵ In this work, ion-water clusters were included to examine the many-body effect, and ion-ion homodimers were included to mainly serve as restraints on CT and CP parameters. The results for alkali metal ions are shown in Figure 2. Good agreement on total energy and energy components was achieved for all ion-water dimers except Li-water dimer. For Li-water dimer, the total energy around the minimum is too low and the equilibrium distance is underestimated. The errors are mainly due to short-range induction energy. For ion-ion homodimers, a reasonable agreement was also achieved. The Na-Na repulsion from AMOEBA+ is weaker than the repulsion from QM, which can be attributed to more favorable induction energies in AMOEBA+. The errors are mainly because of the tradeoff between matching QM energies and experimental HFEs. For ion-water cluster interaction energy, better accuracy was achieved for larger ions K+, Rb+ and Cs+. The magnitude of these cluster interactions for alkali metals is systematically overestimated by AMOEBA+. In general, AMOEBA+ is capable of capturing ion-water and ion homodimer energy components and ion-water cluster interactions for alkali metals, but the accuracy for the gas-phase interactions of some ions needs to be sacrificed to achieve better accuracy for ion pairs and ion HFE. The accuracy in gas-phase interactions is similar to that of the revised AMOEBA parameter (Figure. S1).

Halogen ion interactions are more complex than those of alkali metals due to the diffusive electron cloud. For the halogen ion-water dimer, the minimum energy and the equilibrium distance were reasonably reproduced by AMOEBA+ (Figure 3). The energy components of Cl/Br/I-water dimer interactions were also close to the SAPT results, while errors were found in some energy components of the F-water dimer. For the halogen ion homodimers, one interesting observation is that the short-range electrostatics interaction is attractive. For Cl-/Br-/I-, the electrostatic energy even becomes favorable (negative) at a short distance. The trends for Cl-/Br-/I- were captured by AMOEBA+, while there is a more significant error in the electrostatic energy of F-. The favorable electrostatic interaction between halogen anions is an example of the charge-penetration effect.

Most fixed-charge force fields and AMOEBA represent the electrostatic interactions of anions by point charges or multipoles, so the electrostatic energy will always be unfavorable. The data of halogen ion homodimer is important for the charge-transfer parameters. Preliminary results showed that if the homodimers were not included, the resulting charge-transfer parameters could lead to artificially strong attraction between the anions at a short distance. For the ion-water cluster interactions, larger percentage errors were found in small F-water clusters and large I-water clusters. Again, these are tradeoffs made to reproduce ion pair interaction and HFEs. Contrary to the case of alkali metals, the magnitude of ion-water cluster interactions for halogen ions was systematically underestimated by AMOEBA+. Overall, AMOEBA+ accurately represents both the total energy and energy components of the halogen-water dimer, halogen homodimer and halogen-water clusters, except for the energy components for F- and the ion-water cluster energies for F- and I-. Compared to AMOEBA, the accuracy for halogen ions is much improved (Figure S2).

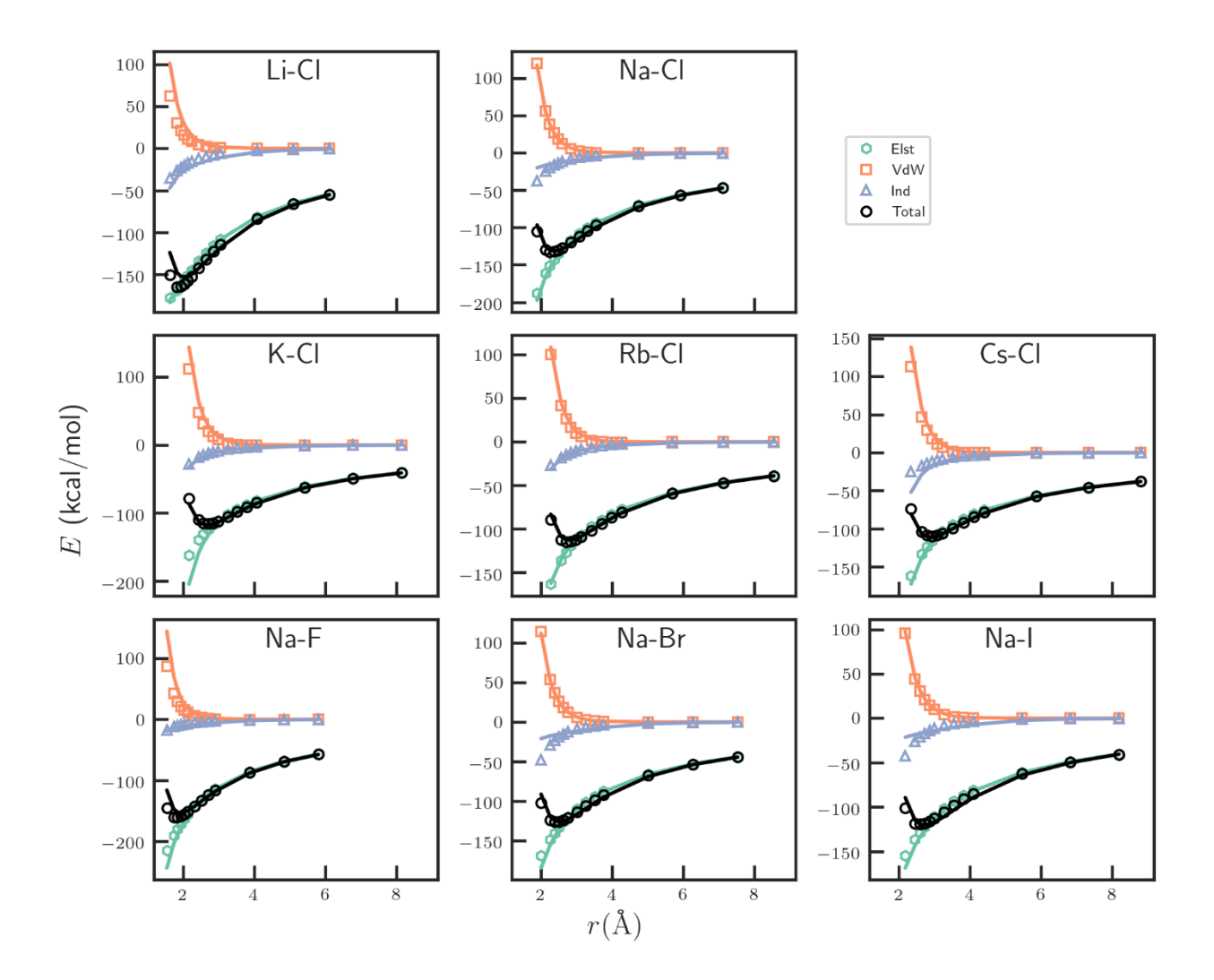


Figure 4: AMOEBA+ and QM interaction energies for cation-anion pairs. QM total interaction energy is calculated by CCSD(T)/CBS, while energy components are calculated by SAPT2+. QM energy is represented as solid lines and MM energy is represented as hollow symbols. See Figure 2 caption for the description of the energy components.

Although gas-phase interactions of ion pairs are much stronger than the interactions in aqueous solution, they are relevant for simulations of high ion concentrations, low dielectric environment and ionic materials. The ion-pair interactions are compared in Figure 4. Similar to the results for ion-water interactions, better agreement with QM was found for interactions without Li+ or F-. AMOEBA+ has higher accuracy for K-Cl, Rb-Cl and Cs-Cl than the revised AMOEBA parameters (Figure S3). Interestingly, the revised AMOEBA is better than the previous AMOEBA for Rb-water and Cs-water interactions but worse for Rb-Cl and Cs-Cl interactions, while

AMOEBA+ is accurate for both the ion-water and ion pair interactions. The interactions of ion pairs Li-Cl and Na-F in AMOEBA+ are stronger than their QM counterpart, with lower minimum energy and shorted equilibrium distance. Li-Cl, Na-F and Cs-Cl have a relatively large error in electrostatics interaction, which is consistent with the large error for homodimers and ion-water dimers of Li+, F-, and Cs+. These trends suggest that the charge-penetration model can capture QM energies for different systems while it is challenging to reproduce both QM energy and experimental ion HFEs.

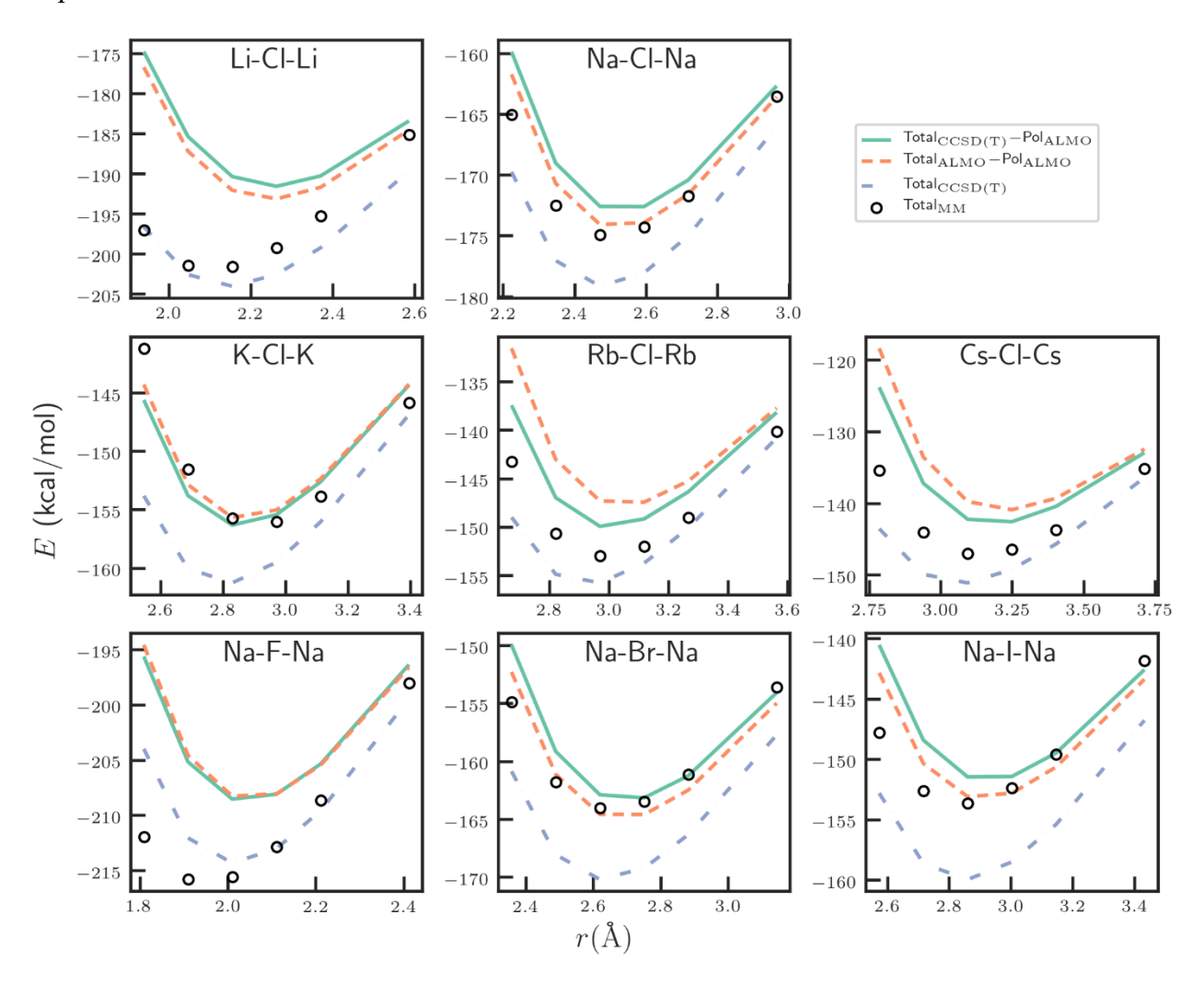


Figure 5: AMOEBA+ and QM interaction energies for symmetric linear ion trimers. QM energy is represented as lines and MM energy is represented as hollow symbols. AMOEBA+ has essentially zero polarization energy for these structures due to symmetry. AMOEBA+ total energy is compared to QM CCSD(T) total energy as well as QM energy excluding polarization using two decomposition schemes, CCSD(T) Total – ALMO Polarization, and ALMO (Total – Polarization).

Symmetric linear ion trimers were included as model systems for weak polarization. Other systems for ion-pair interactions are ion pair dimer and ionic crystals, which have strong and no polarization in AMOEBA, respectively. Therefore, the linear ion trimer systems help prevent overfitting to experimental lattice energies of ionic crystals. Due to symmetry, there is no induced dipole on the anion. The induced dipole on the cations is also negligible. So, AMOEBA+ polarization energy for these trimers is essentially zero. However, there are still induced quadrupole on the central anion in QM treatment, which is missing in AMOEBA+. To characterize the performance of AMOEBA+ non-polarization components, we deducted the polarization energy (beyond induced dipole) from the QM energy. The CCSD(T) total interaction energy and the non-polarization energies calculated by CCSD(T) and/or ALMO were compared with AMOEBA total interaction energy in Figure 5. The CCSD(T) total energy minus ALMO polarization energy was used as the target in parameter optimization while using ALMO nonpolarization energy will produce similar results. For the trimers without Li+ or F-, AMOEBA+ total energy is either close to the QM non-polarization energy or between QM total and nonpolarization energies; compared to QM non-polarization energy, the error in minimum energy is smaller than 5 kcal/mol or 4% and the error in equilibrium distance is smaller than 0.2 Å. For trimers with Li+ or F-, the AMOEBA+ interaction energy is lower than QM non-polarization energy. The errors for Li+ and F- can be attributed to their soft vdW repulsion, which was necessary for reproducing ion-water cluster interactions and HFE. The agreement between AMOEBA+ and QM non-polarization energy for the linear trimers is similar to the results of ion pairs. The lack of induced quadrupole in AMOEBA+ leads to weaker total interaction for some ions and compensates for the error in dimer interaction for other ions such as F- and Li+.

Table 5: Experimental and AMOEBA+ lattice parameters and lattice energies for salt crystals at 0 K.^{40, 43} "dev." means deviation of AMOEBA+ from the experiment.

	a (Å)			L.E. (kcal/mol)		
	Expt.	AMOEBA+	dev.	Expt.	AMOEBA+	dev.
LiF	3.992	3.731	-0.261	-250.7	-266.0	-15.3
LiCl	5.078	5.024	-0.054	-206.5	-207.3	-0.8

LiBr	5.426	5.393	-0.033	-196.0	-195.7	0.3
LiI	5.902	5.846	-0.056	-182.6	-183.3	-0.7
NaF	4.590	4.613	0.023	-222.3	-219.1	3.2
NaC1	5.578	5.719	0.141	-188.8	-187.7	1.1
NaBr	5.908	6.056	0.148	-180.2	-179.5	0.7
NaI	6.388	6.548	0.160	-168.5	-168.0	0.5
KF	5.296	5.428	0.132	-198.1	-196.7	1.4
KC1	6.232	6.435	0.203	-172.1	-171.6	0.5
KBr	6.524	6.745	0.221	-165.2	-163.8	1.4
KI	6.978	7.152	0.174	-155.4	-155.4	0.0
RbF	5.578	5.569	-0.009	-190.0	-190.2	-0.2
RbCl	6.518	6.681	0.163	-166.1	-167.7	-1.6
RbBr	6.820	6.991	0.171	-159.7	-162.6	-2.9
RbI	7.256	7.244	-0.012	-151.1	-154.6	-3.5
CsF	5.964	5.861	-0.103	-181.4	-182.9	-1.5
CsCl	4.068	4.170	0.102	-160.1	-162.3	-2.2
CsBr	4.235	4.203	-0.032	-154.6	-160.7	-6.1
CsI	4.510	4.445	-0.065	-146.5	-152.5	-6.0

The lattice energies are important for the calculation of ionic materials and high concentration ion solutions. Previous work of Wang⁴⁰ suggested that the inclusion of experimental lattice energy in the parameter optimization helps avoid the unphysical ion aggregation in concentrated KCl solutions. Due to the symmetry, the ionic crystals have essentially no polarization (no induced dipole, quadrupole, or octuple), which are very different from ion-water dimers and ion pairs. It plays a similar role for parameter optimization as the linear ion trimer data. The lattice parameters and lattice energies computed by the optimized parameters and the experimental values are tabulated in Table 5. Only crystals containing Na or Cl were used in the parameter fitting, and other crystals are for validation. The largest deviations in lattice parameters are found for LiF, KCl, and KBr. All other lattice parameters are within 0.2 Å of experimental values. The largest deviations in lattice energies are found for LiF, CsBr, and CsI. Compared to the revised AMOEBA ion parameters of Wang,⁴⁰ lattice energies for Li/F-containing crystals and some lattice parameters were improved, while the lattice energies for other crystals are slightly worse. The current work does not have special pairwise vdW parameters as used in the revised

AMOEBA parameter.⁴⁰ These results demonstrate that AMOEBA+ has good performance for both gas-phase and crystals without using special parameters. Since there is no polarization in the crystals, the remaining error likely comes from the functional forms or combining rules of charge transfer and vdW.

Table 6: Experimental and AMOEBA+ ion hydration free energies (kcal/mol). "dev." means deviation of AMOEBA+ from Schmid value. The AMOEBA+ uncertainties are 0.2~0.3 kcal/mol.

	Schmid ⁴⁴	Marcus ⁴⁵	Tissandier ⁴⁶	AMOEBA+	dev.
F	-119.74	-114.96	-104.39	-120.19	-0.45
Cl	-89.15	-85.09	-74.61	-89.35	-0.20
Br	-82.70	-79.11	-68.20	-82.95	-0.25
Ι	-74.33	-69.55	-59.26	-74.48	-0.15
Li	-113.77	-117.35	-128.43	-111.37	2.40
Na	-88.67	-91.06	-103.19	-88.37	0.30
K	-71.22	-74.33	-86.03	-71.15	0.07
Rb	-65.97	-69.55	-80.60	-65.68	0.29
Cs	-60.00	-63.58	N/A	-59.72	0.28

Ion HFE is a very important property for biomolecular simulations, as it contributes to ion binding free energies. Ion hydration is frequently used to explain ion selectivity. ¹² While the relative HFE between ions with the same charge can be determined accurately, several scales for absolute ion HFE exist. ³⁸ The Schmid values ⁴⁴ were chosen as the target as they are in line with the intrinsic HFE from MD simulations of periodic boxes. ¹⁵ Preliminary optimization without the HFE resulted in 1~2 kcal/mol error for Na+, Rb+ and I- and 6 kcal/mol error for Li+. The inclusion of HFE in the target leads to larger errors in some ion-water cluster energies and energy components of ion-ion and ion-water interactions. The HFEs of all ions except Li were reproduced by the optimized parameters (Table 6). For Li, the HFE is smaller than the experiment, while the interaction energies, including Li-water and Li-Cl, and LiCl lattice energies, were all larger than the reference QM or experimental data. This indicates a limitation of current functional forms in describing short-range polarization, charge transfer and/or many-body effect of Li+.

The mean ionic activity coefficients for NaCl and KCl solutions were used as validation. Unphysical salt aggregation was observed in simulations of KCl solution using earlier AMOEBA and fixed-charge force fields, 40 which is related to ionic activity coefficient. The performance of AMOEBA+ for the activity coefficient is similar to that of the revised AMOEBA force field (amoeba18) with special pairwise vdW parameters (Figure 6 and Figure 7). The predicted NaCl activity coefficient at high concentration deviates from the experimental value, which is likely due to the polarization energy since the non-polarization energy in NaCl crystal is weaker than experiment (Table 5). The KCl activity coefficient at high concentration predicted by AMOEBA+ is significantly better than the earlier AMOEBA force field (amoeba09), although it is still lower than the experimental value. Therefore, MD simulations with the optimized parameters should not suffer from the problem of salt aggregation.

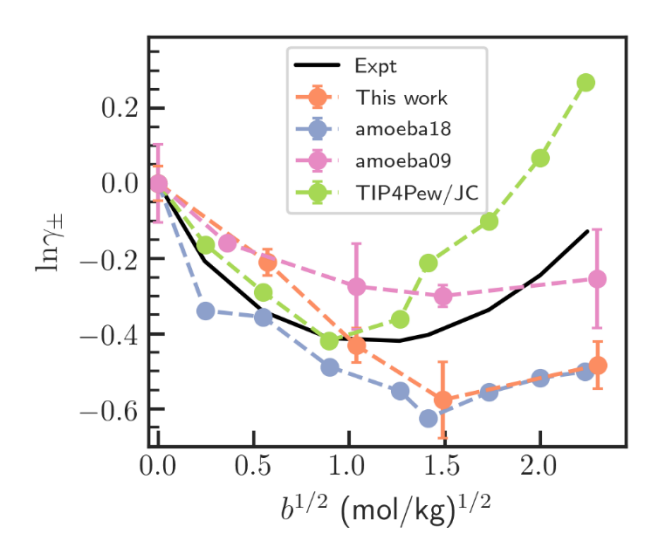


Figure 6: Mean ionic activity coefficient in NaCl aqueous solution from MD simulations with different force fields. "amoeba18" is the revised AMOEBA ion parameters with special pairwise vdW;⁴⁰ "amoeba09" is the earlier AMOEBA parameters of Grossfield et al.¹⁵ Experimental, amoeba18 and TIP4Pew/JC data are taken from Wang.⁴⁰ Error bars represent standard error.

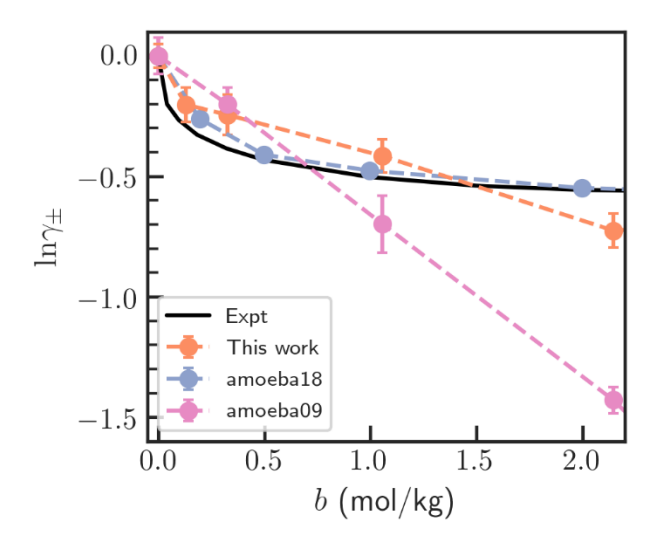


Figure 7: Mean ionic activity coefficient in KCl aqueous solution from MD simulations with different force fields. See Figure 6 caption for description.

4. DISCUSSIONS AND CONCLUSION

The AMOEBA+ force field for alkali metal and halogen ions was developed based on various QM and experimental data. The inclusion of different types of data in the parametrization is both made possible by AMOEBA+ and necessary. The charge penetration model allows for the much-improved description of short-range electrostatics interaction. As a result, the electrostatics energy from QM EDA can be used in the parameterization. Notably, the charge-penetration effect qualitatively alters the trend of short-range electrostatics between halogen ions, which are predicted to be repulsive by point-charge models and attractive by QM and the charge-penetration model. The improved polarization model and the charge-transfer model provide more flexibility for representing the induction energy. The expanded set of parameters also means that more data need to be included in determining the parameters. In AMOEBA, the only adjustable parameters for atomic ions are polarization damping and vdW, and the polarization damping parameters are shared among water, organic molecules and +1/-1 charged ions. By only fitting ion-water dimer interaction energies, AMOEBA could accurately predict HFE. However, AMOEBA ion parameters do not accurately represent some ion-ion interactions, which leads to spurious ion

aggregation in simulations at very high ion concentrations.⁴⁰ On the other hand, different combinations of parameters in AMOEBA+ could reproduce ion-water dimer interactions, and HFE is more sensitive to some parameters than the ion-water interaction is. So AMOEBA+ parameterized solely from ion-water interaction cannot be used to predict HFE. Instead, HFE needs to be included in the parametrization. The necessity for including HFE can also be attributed to the inaccuracy of QM EDA methods and the force field functional forms.

The ion-water cluster interaction is correlated with ion HFE. AMOEBA+ systematically underestimates the magnitude of cation-water cluster interaction while overestimates the magnitude of anion-water cluster interaction. If the sum of ion-pair HFEs rather than individual ion HFEs are used as the target, the ion-water cluster interactions will be better reproduced. Since the physical meaning of experimental ion HFEs is debatable, using the ion pair HFE seems a valid approach. However, this will make cation HFEs smaller than the Schmid value, which is already the smallest among experimental values. Due to uncertainties in QM methods and the force field approximation as well as lack of other evidence supporting a new scale for ion HFE, this work adopted the conventional approach of targeting Schmid value.

AMOEBA+ achieves reasonable accuracy for ion-water and ion-ion interactions, especially for interactions without F-/Li+. The robustness of AMOEBA+ was verified by other properties not included in the parameterization, such as lattice energies of salt crystals and ionic activity coefficients. Compared to fixed-charge force fields and the AMOEBA force field, AMOEBA+ is based on a wider range of reference data; thus it should be more robust and transferable. AMOEBA+ also provides a decomposition of intermolecular force fields which will be helpful for understanding molecular and materials properties.

This work lays the foundation of deriving ion parameters for the AMOEBA+ force field. The protocols used in this work can be applied to develop parameters for other ionic species that have significant charge penetration and charge transfer effects, including the multivalent ions of biological importance,^{7, 16} molecular ions,¹⁴ ionic liquids, and electrolytes⁴⁷ and perovskite systems.⁴⁸

DATA AND SOFTWARE AVAILABILITY

The development version of Tinker used in this work can be found at https://github.com/TinkerTools/tinker-openmm-archive/tree/AMOEBA+CF.

Supporting Information Available: comparison of AMOEBA+ and AMOEBA on ion-water and ion-ion interactions (Figure S1-S3), interaction energies in csv format, structure files in Tinker xyz format and Tinker parameter files.

ACKNOWLEDGMENTS

This work was supported by the National Institutes of Health (Nos. R01GM106137 and R01GM114237), National Science Foundation (CHE-1856173), and CPRIT (RP160657).

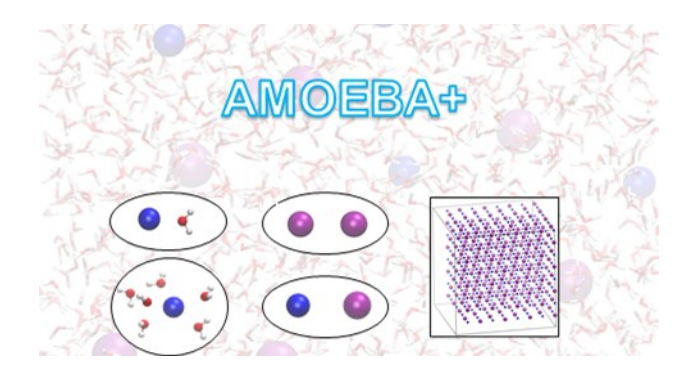
REFERENCES

- 1. Zheng, X.; Cheng, W.; Ji, C.; Zhang, J.; Yin, M., Detection of Metal Ions in Biological Systems: A Review. *Reviews in Analytical Chemistry* **2020**, *39*, 231-246.
- 2. Stelmashook, E. V.; Isaev, N. K.; Genrikhs, E. E.; Amelkina, G. A.; Khaspekov, L. G.; Skrebitsky, V. G.; Illarioshkin, S. N., Role of Zinc and Copper Ions in the Pathogenetic Mechanisms of Alzheimer's and Parkinson's Diseases. *Biochemistry (Moscow)* **2014**, *79*, 391-396.
- 3. Jing, Z.; Qi, R.; Liu, C.; Ren, P., Study of Interactions between Metal Ions and Protein Model Compounds by Energy Decomposition Analyses and the Amoeba Force Field. *J. Chem. Phys.* **2017**, *147*, 161733.
- 4. Cui, Q., Perspective: Quantum Mechanical Methods in Biochemistry and Biophysics. *J. Chem. Phys.* **2016**, *145*, 140901.
- 5. Li, P.; Merz, K. M., Metal Ion Modeling Using Classical Mechanics. *Chem. Rev.* **2017**, 117, 1564-1686.
- 6. Fyta, M.; Netz, R. R., Ionic Force Field Optimization Based on Single-Ion and Ion-Pair Solvation Properties: Going Beyond Standard Mixing Rules. *J. Chem. Phys.* **2012**, *136*, 124103.
- 7. Grotz, K. K.; Cruz-León, S.; Schwierz, N., Optimized Magnesium Force Field Parameters for Biomolecular Simulations with Accurate Solvation, Ion-Binding, and Water-Exchange Properties. *J. Chem. Theory Comput.* **2021**.
- 8. Sengupta, A.; Li, Z.; Song, L. F.; Li, P.; Merz, K. M., Parameterization of Monovalent Ions for the Opc3, Opc, Tip3p-Fb, and Tip4p-Fb Water Models. *J. Chem. Inf. Model.* **2021**, *61*, 869-880.
- 9. Li, Z.; Song, L. F.; Li, P.; Merz, K. M., Parametrization of Trivalent and Tetravalent Metal Ions for the Opc3, Opc, Tip3p-Fb, and Tip4p-Fb Water Models. *J. Chem. Theory Comput.* **2021**, *17*, 2342-2354.

- 10. Chang, T.-M.; Dang, L. X., Recent Advances in Molecular Simulations of Ion Solvation at Liquid Interfaces. *Chem. Rev.* **2006**, *106*, 1305-1322.
- 11. Patel, L. A.; Yoon, T. J.; Currier, R. P.; Maerzke, K. A., Nacl Aggregation in Water at Elevated Temperatures and Pressures: Comparison of Classical Force Fields. *J. Chem. Phys.* **2021**, *154*, 064503.
- 12. Jing, Z.; Liu, C.; Qi, R.; Ren, P., Many-Body Effect Determines the Selectivity for Ca²⁺ and Mg²⁺ in Proteins. *Proc. Natl. Acad. Sci. U. S. A.* **2018**, *115*, E7495-E7501.
- 13. Yu, H.; Whitfield, T. W.; Harder, E.; Lamoureux, G.; Vorobyov, I.; Anisimov, V. M.; MacKerell, A. D.; Roux, B., Simulating Monovalent and Divalent Ions in Aqueous Solution Using a Drude Polarizable Force Field. *J. Chem. Theory Comput.* **2010**, *6*, 774-786.
- 14. Lin, F.-Y.; Lopes, P. E. M.; Harder, E.; Roux, B.; MacKerell, A. D., Polarizable Force Field for Molecular Ions Based on the Classical Drude Oscillator. *J. Chem. Inf. Model.* **2018**, *58*, 993-1004.
- 15. Grossfield, A.; Ren, P.; Ponder, J. W., Ion Solvation Thermodynamics from Simulation with a Polarizable Force Field. *J. Am. Chem. Soc.* **2003**, *125*, 15671-15682.
- 16. Jiao, D.; King, C.; Grossfield, A.; Darden, T. A.; Ren, P., Simulation of Ca2+ and Mg2+ Solvation Using Polarizable Atomic Multipole Potential. *J. Phys. Chem. B* **2006**, *110*, 18553-18559.
- 17. Ngo, V.; Li, H.; MacKerell, A. D.; Allen, T. W.; Roux, B.; Noskov, S., Polarization Effects in Water-Mediated Selective Cation Transport across a Narrow Transmembrane Channel. *J. Chem. Theory Comput.* **2021**.
- 18. Ladefoged, L. K.; Schiøtt, B.; Fedosova, N. U., Beneficent and Maleficent Effects of Cations on Bufadienolide Binding to Na+,K+-Atpase. *J. Chem. Inf. Model.* **2021**, *61*, 976-986.
- 19. Liu, C.; Piquemal, J.-P.; Ren, P., Amoeba+ Classical Potential for Modeling Molecular Interactions. *J. Chem. Theory Comput.* **2019**, *15*, 4122-4139.
- 20. Liu, C.; Qi, R.; Wang, Q.; Piquemal, J. P.; Ren, P., Capturing Many-Body Interactions with Classical Dipole Induction Models. *J. Chem. Theory Comput.* **2017**, *13*, 2751-2761.
- 21. Qi, R.; Wang, Q.; Ren, P., General Van Der Waals Potential for Common Organic Molecules. *Bioorg. Med. Chem.* **2016**, *24*, 4911-4919.
- 22. Ponder, J. W.; Wu, C.; Ren, P.; Pande, V. S.; Chodera, J. D.; Schnieders, M. J.; Haque, I.; Mobley, D. L.; Lambrecht, D. S.; DiStasio, R. A.; Head-Gordon, M.; Clark, G. N. I.; Johnson, M. E.; Head-Gordon, T., Current Status of the Amoeba Polarizable Force Field. *J. Phys. Chem. B* **2010**, *114*, 2549-2564.
- 23. Halgren, T. A., The Representation of Van Der Waals (Vdw) Interactions in Molecular Mechanics Force Fields: Potential Form, Combination Rules, and Vdw Parameters. *J. Am. Chem. Soc.* **1992**, *114*, 7827-7843.
- 24. Liu, C.; Piquemal, J.-P.; Ren, P., Implementation of Geometry-Dependent Charge Flux into the Polarizable Amoeba+ Potential. *J. Phys. Chem. Lett.* **2020**, *11*, 419-426.
- 25. Yang, X.; Liu, C.; Walker, B. D.; Ren, P., Accurate Description of Molecular Dipole Surface with Charge Flux Implemented for Molecular Mechanics. *J. Chem. Phys.* **2020**, *153*, 064103.
- 26. Wang, Q.; Rackers, J. A.; He, C.; Qi, R.; Narth, C.; Lagardere, L.; Gresh, N.; Ponder, J. W.; Piquemal, J.-P.; Ren, P., General Model for Treating Short-Range Electrostatic Penetration in a Molecular Mechanics Force Field. *J. Chem. Theory Comput.* **2015**, *11*, 2609-2618.

- 27. Rackers, J. A.; Wang, Q.; Liu, C.; Piquemal, J.-P.; Ren, P.; Ponder, J. W., An Optimized Charge Penetration Model for Use with the Amoeba Force Field. *Phys. Chem. Chem. Phys.* **2017**, *19*, 276-291.
- 28. Mao, Y.; Loipersberger, M.; Horn, P. R.; Das, A.; Demerdash, O.; Levine, D. S.; Veccham, S. P.; Head-Gordon, T.; Head-Gordon, M., From Intermolecular Interaction Energies and Observable Shifts to Component Contributions and Back Again: A Tale of Variational Energy Decomposition Analysis. *Annu. Rev. Phys. Chem.* **2021**.
- 29. Misquitta, A. J., Charge Transfer from Regularized Symmetry-Adapted Perturbation Theory. *J. Chem. Theory Comput.* **2013**, *9*, 5313-5326.
- 30. Lao, K. U.; Herbert, J. M., Energy Decomposition Analysis with a Stable Charge-Transfer Term for Interpreting Intermolecular Interactions. *J. Chem. Theory Comput.* **2016**, *12*, 2569-2582.
- 31. Lao, K. U.; Schäffer, R.; Jansen, G.; Herbert, J. M., Accurate Description of Intermolecular Interactions Involving Ions Using Symmetry-Adapted Perturbation Theory. *J. Chem. Theory Comput.* **2015**, *11*, 2473-2486.
- 32. Frisch, M. J.; Trucks, G. W.; Schlegel, H. B.; Scuseria, G. E.; Robb, M. A.; Cheeseman, J. R.; Scalmani, G.; Barone, V., Gaussian 16, Revision C.01. **2019**.
- 33. Neese, F.; Wennmohs, F.; Becker, U.; Riplinger, C., The Orca Quantum Chemistry Program Package. *J. Chem. Phys.* **2020**, *152*, 224108.
- 34. Smith, D. G. A.; Burns, L. A.; Simmonett, A. C.; Parrish, R. M.; Schieber, M. C.; Galvelis, R.; Kraus, P.; Kruse, H.; Di Remigio, R.; Alenaizan, A.; James, A. M.; Lehtola, S.; Misiewicz, J. P.; Scheurer, M.; Shaw, R. A.; Schriber, J. B.; Xie, Y.; Glick, Z. L.; Sirianni, D. A.; O'Brien, J. S.; Waldrop, J. M.; Kumar, A.; Hohenstein, E. G.; Pritchard, B. P.; Brooks, B. R.; Schaefer, H. F.; Sokolov, A. Y.; Patkowski, K.; DePrince, A. E.; Bozkaya, U.; King, R. A.; Evangelista, F. A.; Turney, J. M.; Crawford, T. D.; Sherrill, C. D., Psi4 1.4: Open-Source Software for High-Throughput Quantum Chemistry. *J. Chem. Phys.* **2020**, *152*, 184108.
- 35. Qi, R.; Jing, Z.; Liu, C.; Piquemal, J.-P.; Dalby, K. N.; Ren, P., Elucidating the Phosphate Binding Mode of Phosphate-Binding Protein: The Critical Effect of Buffer Solution. *Journal of Physical Chemistry B* **2018**, *122*, 6371-6376.
- 36. Harger, M.; Li, D.; Wang, Z.; Dalby, K.; Lagardère, L.; Piquemal, J.-P.; Ponder, J.; Ren, P., Tinker-Openmm: Absolute and Relative Alchemical Free Energies Using Amoeba on Gpus. *J. Comput. Chem.* **2017**, *38*, 2047-2055.
- 37. Rackers, J. A.; Wang, Z.; Lu, C.; Laury, M. L.; Lagardère, L.; Schnieders, M. J.; Piquemal, J.-P.; Ren, P.; Ponder, J. W., Tinker 8: Software Tools for Molecular Design. *J. Chem. Theory Comput.* **2018**, *14*, 5273-5289.
- 38. Shi, Y.; Beck, T. L., Absolute Ion Hydration Free Energy Scale and the Surface Potential of Water Via Quantum Simulation. *Proc. Natl. Acad. Sci. U. S. A.* **2020,** *117*, 30151-30158.
- 39. Duignan, T. T.; Baer, M. D.; Schenter, G. K.; Mundy, C. J., Real Single Ion Solvation Free Energies with Quantum Mechanical Simulation. *Chem. Sci.* **2017**, *8*, 6131-6140.
- 40. Wang, Z. Polarizable Force Field Development, and Applications to Conformational Sampling and Free Energy Calculation. Washington University in St. Louis, St. Louis, Missouri, 2018.
- 41. Clementi, E.; Raimondi, D. L., Atomic Screening Constants from Scf Functions. *J. Chem. Phys.* **1963**, *38*, 2686-2689.
- 42. Liu, C.; Qi, R.; Wang, Q.; Piquemal, J.-P.; Ren, P., Capturing Many-Body Interactions with Classical Dipole Induction Models. *J. Chem. Theory Comput.* **2017**, *13*, 2751–2761.

- 43. Ghate, P. B., Third-Order Elastic Constants of Alkali Halide Crystals. *Phys. Rev.* **1965**, 139, A1666-A1674.
- 44. Schmid, R.; Miah, A. M.; Sapunov, V. N., A New Table of the Thermodynamic Quantities of Ionic Hydration: Values and Some Applications (Enthalpy–Entropy Compensation and Born Radii). *Phys. Chem. Chem. Phys.* **2000**, *2*, 97-102.
- 45. Marcus, Y., Thermodynamics of Solvation of Ions. Part 5.-Gibbs Free Energy of Hydration at 298.15 K. *Journal of the Chemical Society, Faraday Transactions* **1991**, 87, 2995-2999.
- 46. Tissandier, M. D.; Cowen, K. A.; Feng, W. Y.; Gundlach, E.; Cohen, M. H.; Earhart, A. D.; Coe, J. V.; Tuttle, T. R., The Proton's Absolute Aqueous Enthalpy and Gibbs Free Energy of Solvation from Cluster-Ion Solvation Data. *J. Phys. Chem. A* **1998**, *102*, 7787-7794.
- 47. Bedrov, D.; Piquemal, J.-P.; Borodin, O.; MacKerell, A. D.; Roux, B.; Schröder, C., Molecular Dynamics Simulations of Ionic Liquids and Electrolytes Using Polarizable Force Fields. *Chem. Rev.* **2019**, *119*, 7940-7995.
- 48. Rathnayake, P. V. G. M.; Bernardi, S.; Widmer-Cooper, A., Evaluation of the Amoeba Force Field for Simulating Metal Halide Perovskites in the Solid State and in Solution. *J. Chem. Phys.* **2020**, *152*, 024117.



TOC Graphic

Supporting information for

Advanced electrostatic model for monovalent ions based on *ab initio* energy decomposition

Zhifeng Jing, † Chengwen Liu, † and Pengyu Ren*

Department of Biomedical Engineering, The University of Texas at Austin, Austin, TX 78712

[†] Authors that contributed equally

^{*} Corresponding author. Email: pren@mail.utexas.edu

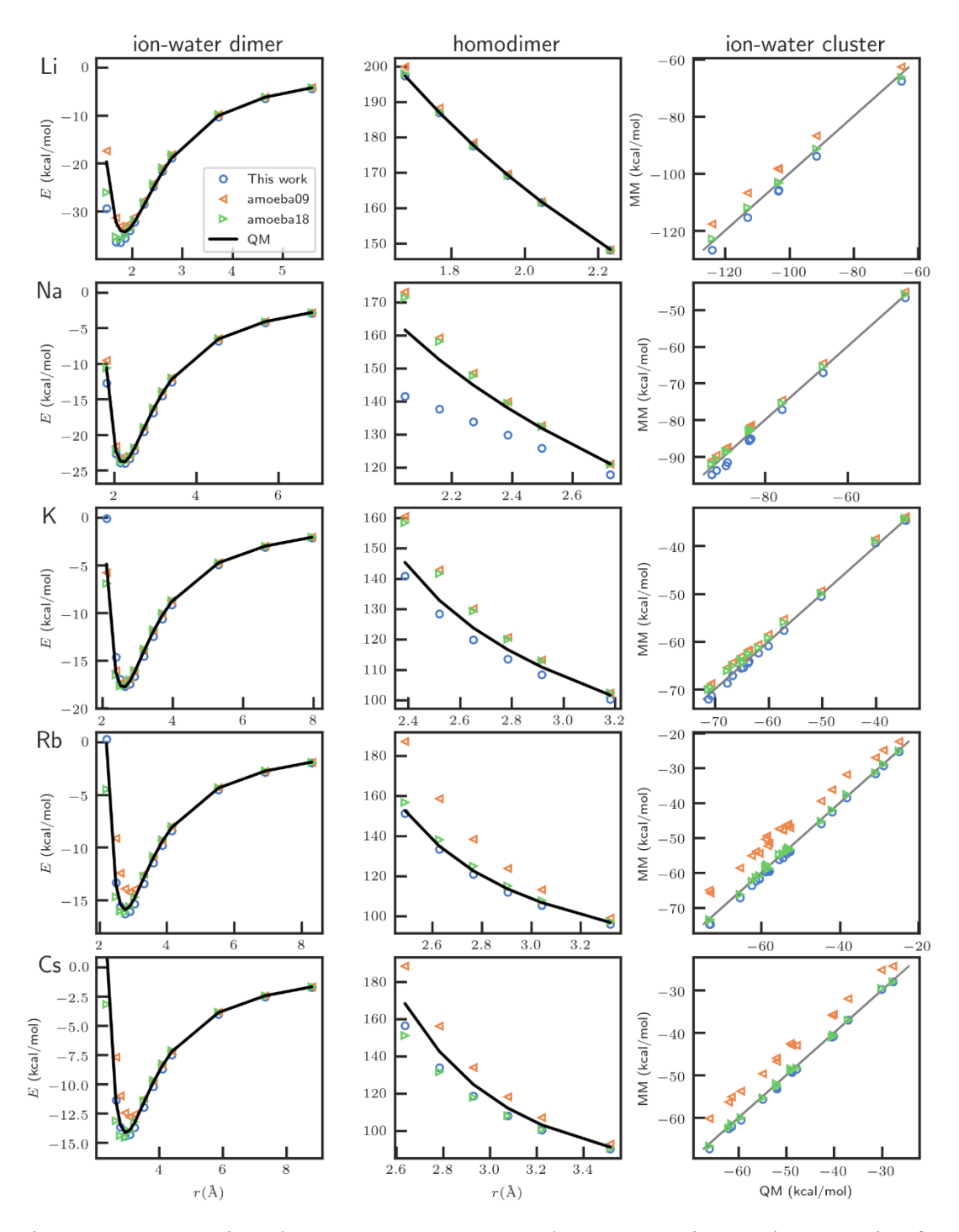


Figure S1. Comparison between AMOEBA+ and AMOEBA interaction energies for Li, Na, K, Rb, and Cs. "amoeba09" includes the Na, K and Cl parameters of Grossfield *et al.*¹ and preliminary parameters for other ions. "amoeba18" is described by Wang.²

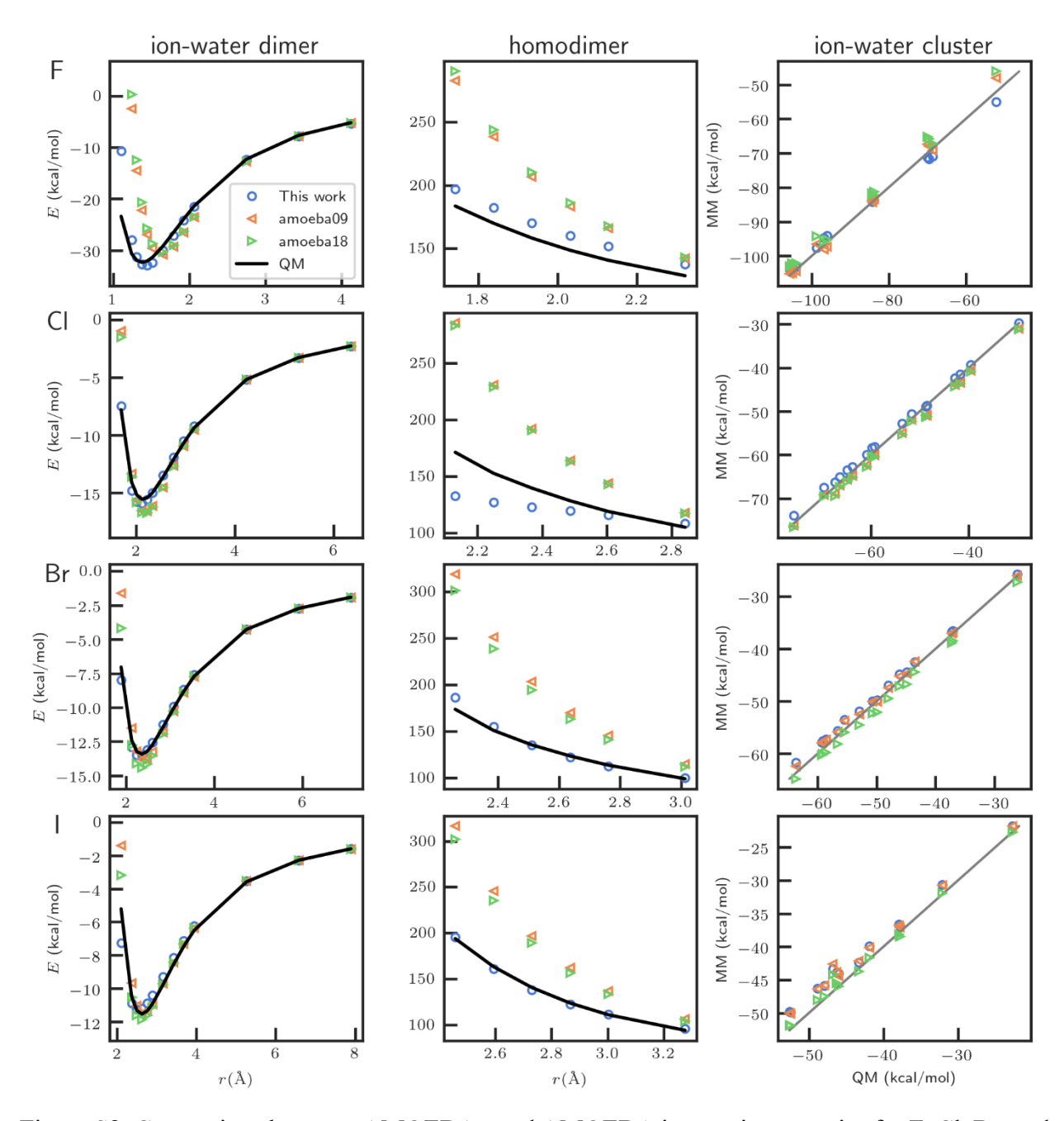


Figure S2. Comparison between AMOEBA+ and AMOEBA interaction energies for F, Cl, Br, and I.

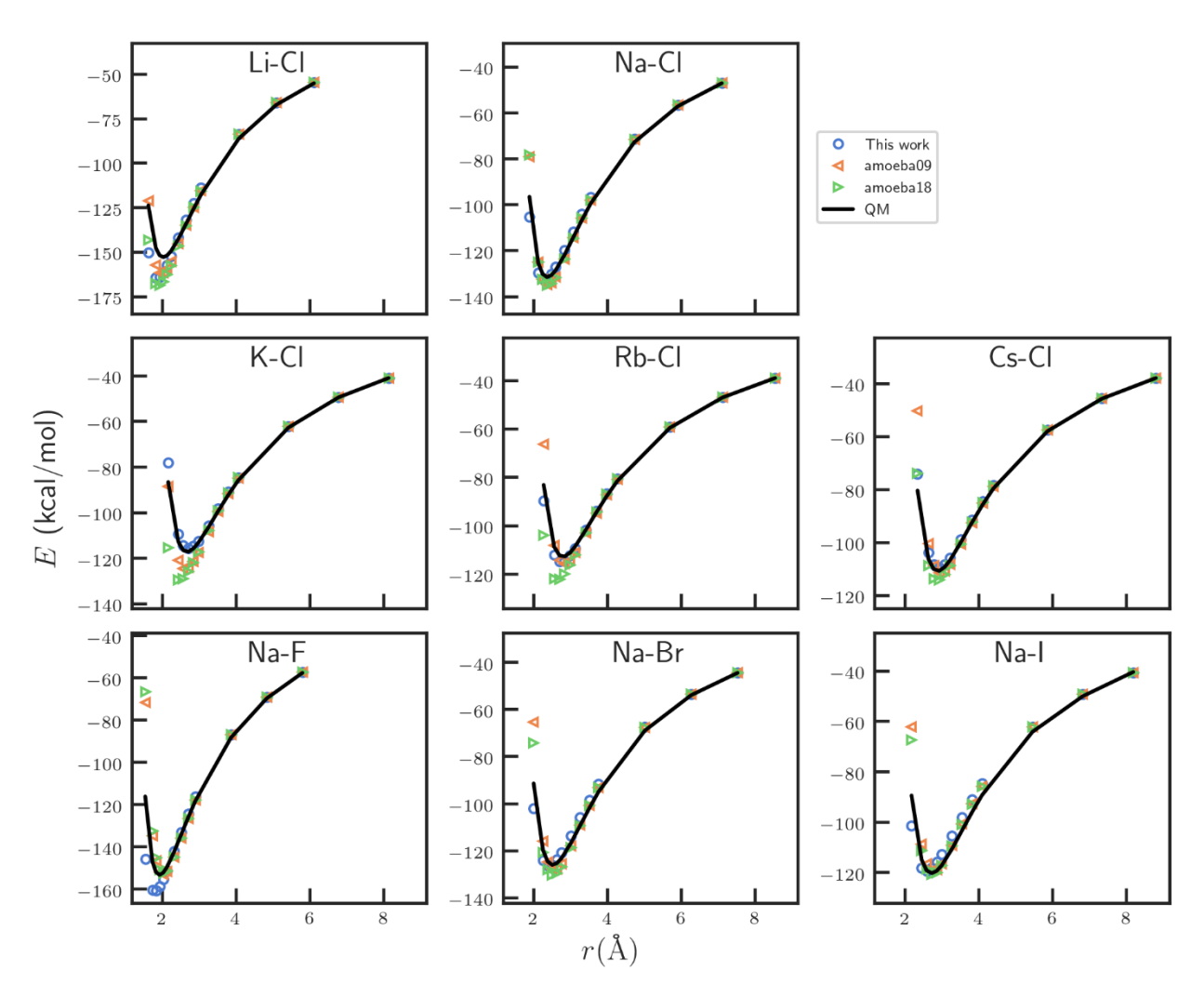


Figure S3. Comparison between AMOEBA+ and AMOEBA interaction energies for ion pairs.

REFERENCES

- 1. Grossfield, A.; Ren, P.; Ponder, J. W., Ion Solvation Thermodynamics from Simulation with a Polarizable Force Field. *J. Am. Chem. Soc.* **2003**, *125* (50), 15671-15682.
- 2. Wang, Z. Polarizable Force Field Development, and Applications to Conformational Sampling and Free Energy Calculation. Washington University in St. Louis, St. Louis, Missouri, 2018.